Isothermal crystallization of anhydrous milk fat in presence of free fatty acids and their esters: From nanostructure to textural properties

Mathilde Bayard[1,2], Brice Kauffmann[3], Jean-Michaël Vauvre[2], Fernando Leal-Calderon[1], Maud Cansell[1]

[1] Université de Bordeaux, CNRS, Bordeaux INP, CBMN UMR 5248, 33600 Pessac, France

[2] Soredab, La Tremblaye, 78125 La Boissière Ecole, France

[3] Université de Bordeaux, CNRS, INSERM, IECB UMS3033, 33600 Pessac, France

* To whom correspondence should be addressed: Maud Cansell,
CBMN, CNRS, UMR 5248, Université de Bordeaux, Bordeaux INP, Allée Geoffroy Saint Hilaire, 33600 Pessac, France
Tel: 33 (0)5 40 00 68 19
e-mail: mcansell@enscbp.fr

Running title: Modulation of anhydrous milk fat crystallization by additives

Key words: anhydrous milk fat; isothermal crystallization; esterified and free fatty acids; multiscale properties.

Abbreviations: AMF Anhydrous milk fat; FFA Free fatty acid; p-NMR pulsed Nuclear magnetic resonance; SFC Solid fat content; SAXS Small angle X-ray scattering, TAG Triacylglycerol; WAXS Wide angle X-ray scattering

Abstract

We performed a multiscale study to understand the impact of pure exogenous compounds at low concentration on the crystallization of triacylglycerols (TAGs) in anhydrous milk fat (AMF). We selected butyric acid, an inhibitor of crystallization, and palmitic acid, a promotor, to investigate the influence of the chain length. Tripalmitin was also used as a promotor to assess the impact of fatty acid esterification. Melted blends containing the additives (1 wt.%) were quenched at 25 °C. X-ray scattering data showed that AMF TAGs crystallized directly in the β'-2L form. The presence of additives did not modify the nanostructure of TAG crystals. However, they significantly altered the microstructure of AMF, as revealed by polarized light microscopy and rheology. This study emphasizes the interest of a multiscale approach to gain knowledge about the behavior of complex fat blends and of the use of modulators at low concentration to monitor their textural properties.

1. Introduction

Triacylglycerols (TAGs), the major lipid species in milk, combine more than 400 fatty acids (FAs) which differ in their chain length, the presence of double bonds or branches, and the cis / trans configuration of the double bonds. The wide spectrum of FAs in milk fat, associated with their distribution in TAGs, make milk fat one of the most complex natural fats, especially for its thermal behavior (Shi, Smith, & Hartel, 2001). At 5°C, and even at room temperature, milk fat consists of a mixture of liquid and solid phases. Mastering the crystallization status of milk fat is of primary importance at it determines for instance its bulk rheological properties and, consequently, the processability of products such as butter (Rønholt, Mortensen, & Knudsen, 2013).

The solid fraction is organized in the form of a crystal lattice, generally described with three levels of organization: the nanostructure (0.4 to 100 nm), the microstructure (0.1 to 100 µm) and the macrostructure (> 100 µm) (Ramel, Peyronel, & Marangoni, 2016). Milk fat crystals are arranged at the nanometer scale in a regular three-dimensional pattern. Two organizational levels in TAG crystals can be distinguished: the transverse mode of packing of the aliphatic chains in TAGs, defining the sub-cell structure leading to the definition of the polymorphic forms, and the hydrocarbon chain packing corresponding to the spatial arrangement of TAG molecules (Metin & Hartel, 2005; Ribeiro et al., 2015). The main form encountered in anhydrous milk fat (AMF) is the orthorhombic β' form (Mazzanti, Guthrie, Sirota, Marangoni, & Idziak, 2004; Ollivon, Relkin, Michon, Kalnin, & Mariette, 2005). However, other metastable polymorphs can be encountered depending on the crystallization conditions. For example, a polymorph, called γ or sub-α, less common and very unstable, can form

67 in AMF at very low temperature (< -8 °C), under rapid cooling rates (> 2.5 °C / min)
68 (ten Grotenhuis, van Aken, van Malssen, & Schenk, 1999; Lambert et al., 2017).
69 Although the structure of AMF is very largely dictated by its TAG composition
70 and its crystallization conditions, minor compounds, *i.e.* endogenous, exogenous
71 molecules, or compounds formed during the cheese process can also influence the
72 crystallization kinetics and the physical characteristics of the fat (Smith, Bhaggan,
73 Talbot, & Malssen, 2011; Talbot, Smith, & Bhaggan, 2012; Rønholt et al., 2013; Sato,
74 Bayés-García, Calvet, Cuevas-Diarte, & Ueno, 2013; Bayés-García et al., 2015;
75 Patel & Dewettinck, 2015; Ribeiro et al., 2015; Bayard, Leal-Calderon, & Cansell,
76 2017). Crystallization of TAGs is usually described as a combination of two
77 processes: nucleation, corresponding to the formation of TAG nano-aggregates, and
78 crystalline growth during which liquid TAG molecules are incorporated at the surface
79 of stable nuclei (Metin & Hartel, 2005; Ribeiro et al., 2015). Minor compounds can
80 influence each of these processes. They can promote heterogeneous nucleation
81 (Rønholt et al., 2013; Sato et al., 2013; Bayés-García et al., 2015; Bayard et al.,
82 2017) or prevent it (Smith et al., 2011; Sato et al., 2013; Bayard et al., 2017). Minor
83 compounds can also accelerate or inhibit crystal growth (Metin & Hartel, 2005; Smith
84 et al., 2011; Talbot et al., 2012; Bayard et al., 2017). Their influence on nucleation
85 and growth can be antagonistic, accelerating one and slowing the other (Talbot et al.,
86 2012). The presence of minor compounds may thus modify the crystalline
87 microstructure of neat AMF changing the size, the shape and/or the volume density
88 of crystals (Bayard et al., 2017). Finally, minor compounds can direct fat
89 polymorphism, in particular by inhibiting some polymorphic transitions. This can be
90 explained by the increase in the liquid fraction during solid-solid polymorphic
91 transitions. They could also act by poisoning growth sites during recrystallization in

92 polymorphic phase transitions between solid forms involving crystal melting (Smith et
93 al., 2011; Talbot et al., 2012). The various effects of the modulators on crystallization
94 and on the resulting physical properties of AMF are very dependent on their chemical
95 nature (Wright & Marangoni, 2003; Smith et al., 2011), their concentration
96 (Vanhoutte, Dewettinck, Foubert, Vanlerberghe, & Huyghebaert, 2002; Foubert,
97 Vanhoutte, & Dewettinck, 2004), and the processing conditions (Sato et al., 2013;
98 Kaufmann, De Graef, Dewettinck, & Wiking, 2012). Despite the considerable interest
99 on AMF motivated by its wide use in food products, the interactions between AMF
100 and other non-TAG lipids are still poorly understood. Only few studies deal with the
101 effect of endogenous or exogenous minor compounds in milk fat crystallization and
102 the reported results are not always consistent. According to some studies, removing
103 polar compounds accelerates crystallization (Wright, Hartel, Narine, & Marangoni,
104 2000; Mazzanti et al., 2004), while in other studies, crystallization is delayed
105 (Herrera, de León Gatti, & Hartel, 1999). Instead of removing endogenous minor
106 compounds, it may be worthwhile to add specific molecules. Phospholipids were
107 shown to delay the onset time of AMF isothermal crystallization (Vanhoutte et al.,
108 2002). Addition of diglycerides to AMF slowed crystallization (Wright et al., 2000;
109 Wright & Marangoni, 2002) without modifying the microstructure (Wright &
110 Marangoni, 2003). At 25 °C, the addition of diolein accelerated crystallization of AMF,
111 while distearin slowed it down (Foubert et al., 2004). Addition of a blend of mono and
112 diglycerides to AMF favored crystallization, that occurred at a higher temperature
113 than in the absence of these partial glycerides (Ollivon et al., 2005; Foubert et al.,
114 2004; Wright et al., 2000; Wright & Marangoni, 2002; Wright & Marangoni, 2003).
115 Depending on the temperature and their concentration, mono-olein and mono-stearin
116 could either accelerate or delay AMF crystallization (Foubert et al., 2004). Such

117 contradictory results could be explained, at least partly, by the variability in the
118 composition of milk fat both in terms of endogenous minor species and/or FA
119 proportions due to seasonal variations.
120 Recently, we studied the impact of various free FAs (FFAs) and of some of their
121 derivatives on isothermal crystallization of AMF at 25 °C (Bayard et al., 2017). Such
122 crystallization conditions are relevant since many food products containing milk fat
123 are stored at constant temperature after being processed. Moreover, the temperature
124 of 25 °C was selected because it provided exploitable kinetic data over a reasonable
125 time scale and because it allowed to better reveal the impact of modulators (Smith et
126 al., 2011). We showed that, depending on the FA chain length and/or unsaturation,
127 FFAs can either promote or inhibit AMF crystallization. The crystallization kinetics
128 were characterized by proton NMR. The kinetic evolution of crystallization was
129 modelled using Gompertz (1825) model based on 3 parameters: the induction time,
130 the final solid fat content and the maximal crystallization rate. Nevertheless, p-NMR
131 technic actually does not provide direct structural information. Here, we implement a
132 structural and mechanistic multiscale approach aiming to decipher the mechanisms
133 of action of some of these modulators on the molecular organization of FAs and
134 TAGs in AMF. We selected two antagonistic modulators, namely butyric acid (4:0),
135 an inhibitor of crystallization, and palmitic acid (16:0), a promotor, to investigate the
136 influence of the chain length. The study also integrated tripalmitin, a promotor, to
137 assess the impact of esterification. We combine a nanoscale study based on X-ray
138 scattering with a microstructure study using polarized microscopy. Finally, we
139 investigated the impact of the microstructure on the textural properties of AMF in
140 presence of the modulators.
141

2. Materials and Methods

2.1. Materials

AMF was supplied by Corman SA (Goé, Belgium) and used without further purification. AMF fatty acid composition was determined by gas chromatography. It was composed of approximately 6% short chain FAs (strictly less than 8 carbons), 20% midsize chains and 72% long chains (strictly more than 14 carbons), including 42% saturated 16 and 18 chains. Unsaturated chains represented 27% of the total FAs, oleic acid being the most abundant one. Palmitic acid (16:0, purity ≈ 98%, M = 256 g/mol), butyric acid (4:0, purity > 97%, M = 116 g/mol), and tripalmitin (purity > 85%, M = 807 g/mol) were purchased from Sigma Aldrich (Saint-Quentin Fallavier, France).

2.2. X-ray diffraction

X-rays were generated by a rotating copper anode (MM07, Rigaku) with a power of 1.2 kW, at a wavelength λ = 1.54187 Å. The melted fat sample was placed on a nylon loop as sample holder and centered on the source. It was thermostatically controlled by a flow of nitrogen (Cryostem, Oxford). The detector was a curved plate screen placed at a distance D from the sample. The sample was exposed for 10 min during which it rotated 180 °. X-rays were diffracted at 2θ angles corresponding to the distances between the planes of atoms in the crystals. A diffraction pattern of concentric circles was thus obtained. After subtracting the signal from the sample holder, and integrating the intensity of the signal over the entire diffraction circle, a one-dimensional signal, depending only on the diffraction angle, was obtained. It is

usually represented as a function of the reciprocal space variable $q = 2\pi / d$, d being the distance separating two diffracting planes.

To follow the kinetics of crystallization, the sample holder was initially immersed in melted fat (AMF with or without modulators) and maintained at 60 °C for 10 min. Acquisition at this temperature ensured that the mixture was completely melted. Then, the temperature of the sample was set at 25 °C. Each plate acquisition and reading lasted 10 min, the time which then separated the points of the kinetics. The diffractograms were normalized by the area of the signal at t = 0 min, where the fat was completely melted. The peaks were manually integrated by the trapezoid method. A straight line was drawn between the onset and offset wavelengths of the peaks and the area between this line and the signal was measured. The peaks were assigned to reticular distances d and indexed to determine the polymorphic shape of the crystals.

As the device used in this work was configured for wide angle X-ray scattering (WAXS) measurements, it was not suitable to observe distances greater than 30 Å ($q < 0.20$ Å^{-1}) because the detection screen was close to the sample and the beam stop which protected it from non-diffracted X-rays masked the signals corresponding to small diffraction angles. It was therefore not possible to observe the elementary line (Miller index l = 1) which would correspond to the longitudinal stacking distance of the triglycerides. However, it was possible to determine this value owing to the peaks corresponding to higher diffraction orders. Short reticular distances (WAXS) and long reticular distances (small angle X-ray scattering) (SAXS) were studied separately and the peaks were assigned using data from the literature (Lopez, Lavigne, Lesieur, Bourgaux, & Ollivon, 2001; Mazzanti, et al., 2004; Lambert et al., 2017).

The three modulators (butyric acid, palmitic acid and tripalmitin) were added to AMF at 1 wt.%. All systems were previously melted at 80 °C (5 °C higher than the melting temperature of the modulator with the highest melting point) before crystallization. The samples were analyzed in triplicate for neat AMF and the wavelength of the characteristic peaks was reproducible with 1% and the peak intensity within 5%.

2.3. *Polarized-light microscopy*

Crystallized AMF with or without modulators were observed under polarized light. Crossed analyzers were used to polarize light so as to reveal birefringent crystals. The samples were preheated at 85 °C. A drop was placed on a preheated microscope slide and covered with a preheated cover slip. Then, the samples were transferred into a temperature-controlled area at 25 °C. After 4 hours of crystallization, samples were imaged with a polarized light microscope (BX53F, Olympus), equipped with a temperature-controlled Peltier system (T95 PE 120, Linkam). Images were acquired using a 10.6-megapixel digital color camera (SC100, Olympus). The microscopy images were quantitatively processed to determine the number and size of the crystals. After image processing using filters, the contours of the crystals were automatically detected using an internal program (Matlab, Mathworks), the area of each crystal was calculated, and then expressed in equivalent disk diameter to avoid the biases linked to the non-sphericity of the crystals. For each sample, at least 250 crystals were analyzed.

2.4. Pulse nuclear magnetic resonance analysis

Isothermal crystallization of pure AMF and of the various blends was studied at 25 °C by a low field pulse nuclear magnetic resonance (p-NMR) unit equipped with a

215 temperature-controlled measuring probe (Minispec mq20, Bruker, Karlsruhe,
216 Germany) as described in Bayard et al. (2017). To check the repeatability of the
217 measurements, neat AMF was analyzed in triplicate. Differences between the three
218 analyses were always lower than 0.3 solid fat content (SFC) units. The modified
219 Gompertz model used for the determination of the induction time, the final solid fat
220 content and the maximal crystallization rate is described in Bayard et al. (2017).
221
222 *2.5. Rheology measurements*
223 Many studies have demonstrated that AMF exhibits viscoelastic behavior at small
224 stresses (Wright et al., 2001). Viscoelasticity can be probed by evaluating the
225 relationships between stress, strain, and time, using small deformations. AMF and
226 the mixtures were analyzed using a Mars III Thermo Fisher rheometer equipped with
227 a ribbed Duvet cell geometry (CCB / CC16 DIN S), with an internal diameter of 15.7
228 mm, an external diameter of 17 mm, and a height of 23.6 mm. The ridges of the
229 geometry prevented sample slippage on the walls. The temperature was regulated by
230 a Peltier module. Measurements were carried out in the oscillatory regime. In this
231 technique, the apparent complex shear modulus (G*) is determined by applying a
232 small sinusoidal strain, γ, and by measuring both the response in terms of applied
233 stress and phase lag between the periodic strain and stress curves. G* includes a
234 real and an imaginary part that corresponds to the storage (G') and loss (G'')
235 modulus, respectively. For small amplitudes of the deformation, γ_0, the crystallized
236 system was deformed without flowing. In this regime of linear deformation, the shear
237 modulus was almost constant whatever the deformation. A sweep in γ_0 at 25 ° C was
238 performed to determine this linear zone. The scans were carried out with γ_0 varying
239 between 10^{-4} and 10, at a frequency of 1 Hz (pulse of 2π). To remain in the linear

240 regime, the working amplitude was fixed at 0.001. In the linear rheological regime
241 adopted here, samples were submitted to a sinusoidal perturbative shear that is
242 supposed not to alter the microstructure. Although rheology samples are being
243 sheared, it is generally admitted that only minor local rearrangements occur under
244 such experimental conditions, allowing a comparison with p-NMR and XDR where
245 samples are completely at rest. AMF with and without the modulators was previously
246 melted and introduced into the cell at 60 °C. A temperature ramp at -5 °C/min was
247 applied until 25 °C was reached. Crystallization was then followed for 2 h. The
248 samples were analyzed in triplicate and the final rheological moduli were
249 reproducible within 20%.
250
251 *2.6. Statistical analysis*
252 Crystal sizes were expressed as mean values with standard deviation (mean ± SD).
253 Comparisons were analyzed using a one-way analysis of variance followed by a
254 pairwise t-test using R version 3.1.2 (Rcommander package). Differences with P-
255 values <0.05 were considered to be statistically significant.
256
257 **3. Results and discussion**
258 Despite numerous studies conducted on the impact of endogenous or added
259 components on fat crystallization and on the mechanism of crystal nucleation and
260 growth (Ribeiro et al., 2015; Sato et al., 2013; Smith et al., 2011), only very few of
261 them deal with the addition of a pure TAGs into a fat blend (Basso et al., 2010;
262 Vereecken, Foubert, Smith, & Dewettinck, 2009).
263 In a previous study, we have shown, using p-NMR measurements and microscopy
264 observations, that exogenous FFAs and TAGs modulated the kinetics of

crystallization of AMF (Bayard et al., 2017). However, only hypotheses could be provided concerning the potential nanostructures and the consequences on the macrostructure were not investigated. Thus, the objective of the present study is: (1) to extent the NMR study to butyric acid, (2) to characterize the nanostructure of AMF blends in order to better understand the role of modulators on AMF polymorphism, (3) to analyze the obtained crystals, and (4) to correlate the results obtained at the nano and microscales to the rheological behavior of AMF and its blends. We adopted a similar experimental approach as in Bayard et al. (2017), based on the addition of high purity modulators, and isothermal conditions of 25 °C to impose a low undercooling degree, while provoking AMF crystallization in less than 3 hours.

3.1. Effect of free fatty acids and their esters on the nanostructure of AMF during isothermal crystallization at 25 °C

The crystal structure of AMF with and without modulator was studied at the nanoscale, with the characterization of the long and short reticular distances of TAG crystal lattices by X-ray diffraction. Fig. 1 shows the kinetic evolution of the diffractograms of neat AMF during isothermal crystallization at 25 °C. In the melted state, diffraction peaks were observed at 4,5 Å (q=1,4 $Å^{-1}$) and 22 Å (q=0,28 $Å^{-1}$), attributed to a liquid-crystalline state (Larsson, 1992; Cebula, McClements, Povey, & Smith, 1992). At wide diffraction angles, as crystallization took place, the broad peak at 4.5 Å decreased and scattering peaks appeared, corresponding to the progressive spatial organization of the FA chains of TAGs at 25 °C. The peaks at 3.84 Å and 4.27 Å correspond to the polymorphic β' form. The shoulder at 4.12 Å could be due to the α form. The peak at 4.38 Å was attributed to a polymorphic $β'_2$ form. It is worth noting that at 25 °C, the β' form was formed directly from the melted fat. The examination of

290 long reticular distances measured by SAXS allowed to characterize the spatial
291 organization of TAGs. At small diffraction angles, three peaks corresponding to large
292 reticular distances, namely 20.8 Å, 13.8 Å and 11.48 Å appeared, and their
293 intensities increased with time (Fig. 1). From these values, it was possible to deduce
294 a distance of 43.8 Å for the first order diffraction peak, corresponding to a lamellar
295 structure with double chain-length organization (2L). The best-defined peaks in
296 WAXS (β' peak at 3.84 Å) and in SAXS ($2L_{003}$ at 13.8 Å) were selected to follow AMF
297 crystallization kinetics (Fig. 2). Both evolutions had a sigmoid shape. Previous
298 studies based on p-NMR also revealed a similar one-step scenario for isothermal
299 crystallization of AMF under low supercooling conditions (Bayard et al., 2017;
300 Herrera et al., 1999; Wright, et al., 2000).
301 Crystallization of AMF was studied in the presence of three different modulators:
302 butyric acid, palmitic acid and tripalmitin. Irrespective of its chemical nature, the
303 addition of a modulator in a low proportion (1 wt.%) did not modify the diffraction
304 pattern of AMF (Supplementary data). In particular, the polymorphic β' form was
305 observed at wide angles with all modulators (characteristic peaks at 3.84 Å and 4.27
306 Å), as well as traces of the α form presumably corresponding to the shoulder at 4.11
307 Å. Similarly, modulators did not alter the 2L organization of TAG molecules ($2L_{003}$ at
308 13.8 Å). The SAXS peak at 38.41 Å (0.16 $Å^{-1}$) with tripalmitin and butyric acid was
309 considered as a part of the peak $2L_{001}$. The evolution of WAXS and SAXS peak
310 intensity remained sigmoidal but varied significantly depending on the modulator
311 nature (Fig. 3A and B). The addition of butyric acid slowed down nuclei formation and
312 decreased the final peak intensity. This behavior was consistent with that of
313 isothermal crystallization observed by p-NMR, with a longer induction time (60.2 min)
314 and a reduced final SFC (9.3 %), compared with neat AMF (34.0 min and 10.3%)

315 (Fig. 4). This behavior was also reported for AMF in presence of other short chain
316 length modulators like propionic (3:0) and hexanoic (6:0) acids (Bayard et al., 2017).
317 Adequation between X-ray diffraction analysis and p-NMR measurements was not so
318 obvious in the presence of palmitic acid. Indeed, compared with AMF, X-ray
319 diffraction did not reveal the promoting effect of this FFA, whereas an acceleration of
320 the crystallization kinetics was observed with p-NMR (Fig. 4). Yet, both techniques
321 indicate that palmitic acid with its longer chain promoted crystallization compared
322 with butyric acid (Fig. 3A and B, and 4). Likewise, there was a discrepancy between
323 the results obtained with the two techniques for tripalmitin. With X-ray diffraction,
324 tripalmitin slowed down crystal formation compared with AMF alone but the peak
325 intensities were similar at the end of the process (Fig. 3A and B). In contrast, with p-
326 NMR, tripalmitin reduced the induction time (28.1 min *vs* 34.0 min for AMF) and
327 increased the final SFC (11.9 % *vs* 11.3 % for AMF) (Fig. 4). Such discrepancies
328 may be due to an intrinsic difference between the techniques: NMR measures the
329 percentage of protons in the solid state, whatever its crystalline form, whereas X-ray
330 diffraction reveals specific crystalline forms. However, both X-ray diffraction and p-
331 NMR revealed differences in the impact of palmitic acid and of its esterified form,
332 tripalmitin, on AMF crystallization. Palmitic acid and tripalmitin favored AMF
333 crystallization, most likely because their alkyl chain lengths are comparable to that of
334 the high melting fraction of AMF TAGs. At 1 wt.%, tripalmitin was more efficient to
335 promote crystallization than its corresponding FFA considering the solid fat content at
336 300 min (11.9 % and 10.0 %, respectively) (Fig. 4). This suggests that TAG additives
337 are more compatible than FFAs with the AMF crystal lattice. The integration of FFAs
338 probably induces some disorder in AMF TAG crystals by introducing vacancies that
339 hinder their optimal growth.

340

341 *3.2. Effect of free fatty acids and their esters on the microstructure of AMF during*
342 *isothermal crystallization at 25 °C*

343 The microstructure was analyzed using polarized-light microscopy. Addition of butyric
344 acid to AMF resulted in fewer (82 crystals/mm^2) and bigger (58.0 ± 36.8 µm) crystals
345 than observed for AMF alone (224 crystals/mm^2, 50.5 ± 20.4 µm, $P<0.05$) (Fig. 5A
346 and B). This reflected a reduced number of growing nuclei in the presence of butyric
347 acid. Nevertheless, the spherulitic form was preserved. These observations agree
348 with the increased induction time and the slower nucleation rate (0.1 min^{-1} *vs* 0.2 min^{-}
349 ^{1} for AMF) observed with p-NMR when butyric acid was added to AMF (Fig. 4).
350 Moreover, the less compact stack of spherulites observed in the presence of this
351 inhibitor suggests that secondary nucleation, i.e., nucleation of a new crystal on the
352 surface of a pre-existing crystal, was inhibited. It can be hypothesized that due to
353 their high polarity, short length saturated FFAs can self-organize into reverse micellar
354 structures (brush configuration) (McClements, 2004) and/or that due to the low
355 melting point of butyric acid, molecules do not form crystal nuclei by their own and
356 thus cannot act as a template for heterogeneous nucleation. Short length saturated
357 FFAs may also exhibit surface-active properties. By adsorbing at the liquid-solid
358 nucleus interface, they could hinder further growth.

359 The impact of tripalmitin on nucleation in AMF was confirmed by microscopic
360 observations (Fig. 5C), as this modulator led to smaller (13.4 ± 5.0 µm) and more
361 abundant spherulites (1095 crystals/mm^2) than AMF alone (224 crystals/mm^2, 50.5 ±
362 20.4 µm, $P<0.05$), reflecting the formation of a larger number of growing nuclei. The
363 templating effect of tripalmitin could be attributed to its higher melting temperature
364 than that of the bulk phase as reported for saturated TAGs (Smith et al., 2011) and

365 could be favored by a similarity in the chain length to those present in AMF facilitating
366 crystal growth (Basso et al., 2010).
367 In presence of palmitic acid, crystals were hardly discernable and formed a granular
368 microstructure (Fig. 5D). This structure reflects a large number of randomly
369 distributed nucleation events. The amphiphilic nature of palmitic acid would allow this
370 fatty acid to self-assemble in reverse micelles in the melted fat. Due to the stacking of
371 the aliphatic chains, the structures resulting from the self-assembly would constitute
372 numerous nucleation sites. When they contribute to the growth of crystals, fatty acids
373 could induce defects in the mesh, creating gaps by occupying the place of
374 triglycerides. Such defects would slow down crystal growth compared with tripalmitin
375 molecules.
376
377 *3.3. Effect of free fatty acids and their esters on the macrostructure of AMF during*
378 *isothermal crystallization at 25 °C*
379 The kinetics of crystallization at 25 ° C was followed by oscillatory rheology with small
380 deformations in order to study the impact of the microstructure on the textural
381 properties of AMF. Milk fat viscoelastic behavior is a result of the 3-dimensional
382 network of fat crystals intimately associated with a continuous oil phase. Fat
383 networks are made of crystals held together by van der Waals forces and the SFC is
384 one of the primary determinants of AMF rheological properties (Rohm & Weidinger,
385 1993; Kaufmann et al., 2012; Macias-Rodriguez & Marangoni, 2020).
386 The evolution of the storage (G') and viscous (G'') modulus during AMF crystallization
387 is shown in Fig. 6A. As fat was completely melted at the beginning of the experiment,
388 the liquid character was predominant: the two moduli were lower than 1 Pa and G''
389 was higher than G'. As crystallization proceeded, the crystals grew and connected

390 with each other forming a continuous network between the two walls of the
391 rheometer's cell. The elastic modulus G' increased sharply due to this percolation
392 phenomenon. The solid nature then became predominant (G' was larger than G'')
393 and the elastic moduli reached very high values at long times (> 10^5 Pa). G' depends
394 on the volume fraction of crystals formed in the liquid bulk phase as well as on their
395 connectivity. The continuous network of fat crystals bears the stress and contributes
396 to the solid or elastic properties (Narine & Marangoni, 1999). Interestingly, G' showed
397 a transition around 100 Pa (Fig. 6A), revealing a two-stage process, which was not
398 observed in p-NMR experiments. This behavior could be due to the evolution of the
399 microstructure. According to Wright et al. (2001), formation of the solid network
400 begins with initial nucleation sites, which grow into larger crystals as additional TAG
401 molecules crystallize. These larger crystals grow into primary particles, which then
402 aggregate into larger clusters, or microstructures that provide the structural building
403 blocks of the fat crystal network. In our case, at the beginning of crystallization (low
404 SFC), the elasticity of the network would be determined by the bonds between
405 crystals within the clusters. During the second step corresponding to a higher level of
406 solid, the elasticity would be controlled by inter-cluster bonds (Shih, Shih, Kim, Liu &
407 Aksay, 1990).
408 Fig. 6B shows the evolution of the elastic modulus when modulators were added.
409 Addition of a short chain FA, like butyric acid, decreased the elastic modulus
410 measured after 120 min (2.45 MPa in presence of the modulator *vs* 15.3 MPa for
411 AMF alone). As nucleation was delayed (see above), so was the percolation process
412 which took 70 min, instead of 20 min for neat AMF. The induction time for percolation
413 was such that the asymptotic value of G' was not reached after two hours.

414 Spherulites being larger, as revealed by Fig. 5B, the number of contacts between
415 them was reduced and the connectivity loss induced lower elasticity values.
416 The addition of palmitic acid and tripalmitin decreased the induction time and
417 increased the final elastic modulus compared with AMF alone (73.8 MPa and 120
418 Mpa in presence of palmitic acid and tripalmitin, respectively *vs* 15.3 MPa for AMF
419 alone). The formation of small and numerous crystals in presence of these
420 modulators (Fig. 5C and D) obviously accelerates the percolation process and leads
421 to a firmer network because it increases the density of links per unit volume. The final
422 value of G' obtained with tripalmitin was 1.6 times larger than that with palmitic acid,
423 in accord with the higher SFC measured in the presence of the esterified modulator
424 (Fig. 4). This result is also consistent with previous observations showing that rapid
425 cooling leads to smaller crystals, a factor which lead to an increase in butter firmness
426 (Parkinson, Sherman, & Matsumoto, 1970; Deman, Gupta, Kloek, & Timbers, 1985).
427 Overall, we provide evidence that the presence of a modulator at a relatively low
428 concentration of 1% has profound consequences for the rheological properties of
429 AMF. In general, the texture of AMF or of butter are monitored by processing
430 conditions, such as cooling rates (Wright et al., 2001). This study reveals that
431 modulators can also be used to alter the microstructure so as to attain desirable
432 textural characteristics.
433

434 **4. Conclusion**

435 The crystallization of AMF and, therefore, its bulk rheological properties are generally
436 controlled *via* its thermal history (processing conditions). Here, we demonstrate that
437 the presence of a modulator at low concentration can also be used as a control
438 parameter to master AMF properties. This study is particularly relevant considering

439 that minor compounds can be added or are likely to be formed *in situ* under the effect
440 of technological processes involving for instance lipolysis. The physical state of fat
441 results from organization at different length scales. X-ray diffraction made it possible
442 to characterize the nanostructure of fat. We used this technique to study AMF during
443 its isothermal crystallization at 25 °C. Scattering data showed that there was no
444 polymorphic transition at this temperature: the fat crystallized directly in the β'-2L
445 form, from the liquid state, and remained stable in the time interval studied. The
446 addition of crystallization modulators at 1 wt.% did not modify the nanostructure but
447 they significantly altered the microstructure of milk fat. There was actually no evident
448 link between the nano and the microstructures. Rheological measurements allowed
449 to correlate the microstructure to textural properties of AMF and its blends. On the
450 whole, our results highlight that crystallization requires a multiscale approach to
451 master fat properties in dairy products.
452

453 **Acknowledgements**

454 The authors acknowledge the French National Association of Technical Research
455 (ANRT) for its financial support through a Ph.D. research grant for M.B
456 (n°2014/0532).
457

458 **Figure captions**

459

460 Figure 1: Kinetic evolution of X-ray diffraction data, expressed as a function of the
461 scattering vector q ($Å^{-1}$), during isothermal crystallization of AMF at 25 °C. Inserts:
462 Zoom of X-ray diffraction patterns at (A) small angles and (B) wide angles.

463

464 Figure 2: Kinetic evolution of the peak areas of the polymorphic form β' (3.84 Å)
465 (solid line) and 2L (13.8 Å) (dotted line) during isothermal crystallization of AMF at
466 25 °C

467

468 Figure 3: Kinetic evolution the peak areas of (A) the polymorphic form β' (3.84 Å) and
469 (B) 2L staking (13.8 Å) during isothermal crystallization of AMF at 25 °C (———), and
470 AMF blends containing 1 wt.% of free fatty acids or esterified derivatives: butyric acid
471 (·····); palmitic acid (- - - - - - -); tripalmitin (— — —).

472

473 Figure 4: Kinetic evolution of the solid fat content (SFC) during isothermal
474 crystallization, at 25 °C, of AMF and AMF blends containing 1 wt.% of free fatty acids
475 or esterified derivatives: AMF (○) and AMF with 4:0 (♦), 16:0 (■), tripalmitin (∗).

476

477 Figure 5: Polarized light microscopy images of AMF crystallized at 25 °C for 4 h.
478 (A) without additive; with addition of (B) 1 wt.% butyric acid, (C) 1 wt.% tripalmitin,
479 and (D) 1 wt.% palmitic acid.

480

481 Figure 6: (A) Evolution of the elastic (G') (———) and viscous (G'') (- - - - - -) moduli
482 during isothermal crystallization of AMF at 25 °C; (B) Evolution of the elastic modulus

(G') during isothermal crystallization, at 25 °C, of AMF (———), and AMF blends containing 1 wt.% of free fatty acids or esterified derivatives: butyric acid (·····), palmitic acid (- - - - - -); tripalmitin (— — —).

References

Basso, R. C., Ribeiro, A. P. B., Masuchi, M. H., Gioielli, L. A., Gonçalves, L. A. G., dos Santos, A. O., Cardoso, L.P., & Grimaldi, R. (2010). Tripalmitin and monoacylglycerols as modifiers in the crystallisation of palm oil. *Food Chemistry*, *122*(4), 1185–1192. https://doi.org/10.1016/j.foodchem.2010.03.113.

Bayard, M., Leal-Calderon, F., & Cansell, M. (2017). Free fatty acids and their esters modulate isothermal crystallization of anhydrous milk fat. *Food Chemistry, 218,* 22-29. https://doi.org/10.1016/j.foodchem.2016.09.042.

Bayés-García, L., Patel, A. R., Dewettinck, K., Rousseau, D., Sato, K., & Ueno, S. (2015). Lipid crystallization kinetics - Roles of external factors influencing functionality of end products, *Current Opinion in Food Science, 4*, 32–38. https://doi.org/10.1016/j.cofs.2015.04.005

Cebula, D.J., McClements, D.J., Povey, M. J. W., & Smith, P. R. (1992). Neutron diffraction studies of liquid and crystalline trilaurin. *Journal of the American Oil Chemists' Society*, *69*, 130–136.

Deman, J. M., Gupta, S., Kloek, M., & Timbers, G.E. (1985). Viscoelastic properties of plastic fat products. *Journal of the American Oil Chemists' Society*, *62*, 1672–1675.

Foubert, I., Vanhoutte, B., & Dewettinck, K. (2004). Temperature and concentration dependent effect of partial glycerides on milk fat crystallization. *European Journal of Lipid Science and Technology*, *106*(8), 531–539. https://doi.org/10.1002/ejlt.200400979.

Gompertz, B. (1825). XXIV On the nature of the function expressive of the law of human mortality, and on a new mode of determining the value of life contingencies. In A letter to Francis Baily, *Philosophical Transactions of the Royal Society of London*, 115, 513–583. https://doi.org/10.1098/rstl.1825.0026

Herrera, M. L., de León Gatti, M., & Hartel, R. W. (1999). A kinetic analysis of crystallization of a milk fat model system. *Food Research International*, *32*(4), 289–298. https://doi.org/10.1016/S0963-9969(99)00083-6.

Kaufmann, N., De Graef, V., Dewettinck, K. & Wiking, L. (2012). Shear-induced crystal structure formation in milk fat and blends with rapeseed oil. *Food Biophysics*, *7*, 308–316. https://doi.org/10.1007/s11483-012-9269-9.

Lambert, A., Bougrioua, F., Abbas, O., Courty, M., El Marssi, M., Faivre, V., & Bresson, S. (2017). Temperature dependent Raman and X-ray diffraction studies of anhydrous milk fat. *Food Chemistry*, *267*, 187–195. https://doi.org/10.1016/j.foodchem.2017.09.006.

Larsson, K. (1992). On the structure of the liquid state of triglycerides. *Journal of the American Oil Chemists' Society*, *69*, 835–836.

Lopez, C., Lavigne, F. Lesieur, P., Bourgaux, C., & Ollivon, M. (2001). Thermal and structural behavior of milk fat. 1. Unstable species of anhydrous milk fat. *Journal of Dairy Science, 84*, 756–766. https://doi.org/10.3168/jds.S0022-0302(01)74531-6.

Macias-Rodriguez, B.A. & Marangoni, A. G. (2020). Rheology and texture of cream, milk fat, butter and dairy fat spreads. In T. Truong, C. Lopez, B. Bhandari, S. Prakash (Eds), *Dairy Fat Products and Functionality* (pp 245-275). Springer, Cham. https://doi.org/10.1007/978-3-030-41661-4_10.

Mazzanti, G., Guthrie, S. E., Sirota, E. B., Marangoni, A. G., & Idziak, S. H. J. (2004). Effect of minor components and temperature profiles on polymorphism in milk fat. *Crystal Growth & Design, 4*(6), 1303–1309. https://doi.org/10.1021/cg0497602.

McClements, D.J. (2004). *Food emulsions: principles, practices, and techniques* (2nd ed.). *CRC Press, Boca Raton*, 632 p. https://doi.org/10.1201/9781420039436

Metin, S. & Hartel, R. W. (2005). Crystallization of fats and oils. In F. Shadidi (Ed.) (6th ed.), *Bailey's Industrial Oil and Fat Products* (pp. 45–76). John Wiley & Sons, Inc.

Narine, S. S. & Marangoni, A. G. (1999). Relating structure of fat crystal networks to mechanical properties: a review. *Food Research International, 32*(4), 227–248. https://doi.org/10.1016/S0963-9969(99)00078-2.

Ollivon, M., Relkin, P., Michon, C., Kalnin, D., & Mariette, F. (2005). Cristallisation de la matière grasse de lait anhydre : influence du polymorphisme et des émulsifiants. *Sciences des Aliments*, *25*(5-6), 397–411. https://doi.org/10.3166/sda.25.397-411.

Patel, A.R. & Dewettinck, K. (2015). Current update on the influence of minor lipid components, shear and presence of interfaces on fat crystallization. *Current Opinion in Food Science, 3,* 65–70. https://doi.org/10.1016/j.cofs.2015.05.010.

554 Parkinson, C., Sherman, P., & Matsumoto, S. (1970). Fat crystals and the flow
555 rheology of butter and margarine. *Journal of Texture Studies, 1*(2), 206–213.
556 https://doi.org/10.1111/j.1745-4603.1970.tb00724.x.
557 Ramel Jr., P. R. R., Peyronel, F., & Marangoni, A. G. (2016). Characterization
558 of the nanoscale structure of milk fat. *Food Chemistry, 203*(15), 224–230.
559 http://dx.doi.org/10.1016/j.foodchem.2016.02.064.
560 Ribeiro, A. P. B., Masuchi, M. H., Miyasaki, E. K., Domingues, M. A. F.,
561 Stroppa, V. L. Z., Oliveira, G. M. de, & Kieckbusch, T. G. (2015). Crystallization
562 modifiers in lipid systems. *Journal of Food Science and Technology, 52*(7), 3925–
563 3946. https://doi.org/10.1007/s13197-014-1587-0.
564 Rohm, H. & Weidinger, K. H. (1993). Rheological behaviour of butter at small
565 deformations. *Journal of Texture Studies, 24*(2), 157–172.
566 https://doi.org/10.1111/j.1745-4603.1993.tb00041.x.
567 Rønholt, S., Mortensen, K., & Knudsen, J. C. (2013). The effective factors on
568 the structure of butter and other milk fat-based products. *Comprehensive Reviews in*
569 *Food Science and Food Safety*, *12*(5), 468–482. https://doi.org/10.1111/1541-
570 4337.12022.
571 Sato, K., Bayés-García, L., Calvet, T., Cuevas-Diarte, M. À., & Ueno, S.
572 (2013). External factors affecting polymorphic crystallization of lipids. *European*
573 *Journal of Lipid Science and Technology*, *115*(11), 1224–1238.
574 https://doi.org/10.1002/ejlt.201300049.
575 Shih, W.-H., Shih, W. Y., Kim, S.-I., Liu, J., & Aksay, I. A. (1990). Scaling
576 behavior of the elastic properties of colloidal gels. *Physical Review A*, *42*, 4772-4439.
577 https://doi.org/10.1103/PhysRevA.42.4427.

578 Shi, Y., Smith, C. M., & Hartel R. W. (2001). Compositional effects on milk fat
579 crystallization. *Journal of Dairy Science, 84*(11), 2392–2401.
580 https://doi.org/10.3168/jds.S0022-0302(01)74688-7.
581 Smith, K. W., Bhaggan, K., Talbot, G., & Malssen, K. (2011). Crystallization of
582 fats: Influence of minor components and additives. *Journal of the American Oil*
583 *Chemists' Society, 88,* 1085–1101. https://doi.org/10.1007/s11746-011-1819-7.
584 Talbot, G., Smith, K., & Bhaggan, K. (2012). Influence of minor components on
585 fat crystallization. *Lipid Technology, 24,* 83–85.
586 https://doi.org/10.1002/lite.201200180.
587 ten Grotenhuis, E., van Aken, G. A., van Malssen, K. F., & Schenk, H. (1999).
588 Polymorphism of milk fat studied by differential scanning calorimetry and real-time X-
589 ray powder diffraction. *Journal of the American Oil Chemists' Society, 76*, 1031–
590 1039. https://doi.org/10.1007/s11746-999-0201-5.
591 Vanhoutte, B., Dewettinck, K., Foubert, I., Vanlerberghe, B., & Huyghebaert,
592 A. (2002). The effect of phospholipids and water on the isothermal crystallization of
593 milk fat. *European Journal of Lipid Science and Technology*, *104*(8), 490–495.
594 https://doi.org/10.1002/1438-9312(200208)104:8<490::AID-EJLT490>3.0.CO;2-U.
595 Vereecken, J., Foubert, I., Smith, K. W., & Dewettinck, K. (2009). Effect of
596 SatSatSat and SatOSat on crystallization of model fat blends. *European Journal of*
597 *Lipid Science and Technology*, *111*(3), 243–258.
598 https://doi.org/10.1002/ejlt.200800150.
599 Wright, A. J., Hartel, R. W., Narine, S. S., & Marangoni, A. G. (2000). The
600 effect of minor components on milk fat crystallization. *Journal of the American Oil*
601 *Chemists' Society*, *77*(5), 463–475. https://doi.org/10.1007/s11746-000-0075-8.

602 Wright, A. J., Scanlon, M. G., Hartel, R. W., & Marangoni, A. G. (2001).
603 Rheological properties of milkfat and butter. *Journal of Food Science, 66*(8), 1056-
604 1071. https://doi.org/10.1111/j.1365-2621.2001.tb16082.x.
605 Wright, A. J. & Marangoni, A. G. (2002). Effect of DAG on milk fat TAG
606 crystallization. *Journal of the American Oil Chemists' Society*, *79*(4), 395–402.
607 https://doi.org/10.1007/s11746-002-0495-5.
608 Wright, A. & Marangoni, A. G. (2003). The effect of minor components on milk
609 fat microstructure and mechanical properties. *Food Engineering and Physical*
610 *Properties*, *68*(1), 182–186. https://doi.org/10.1111/j.1365-2621.2003.tb14137.x.
611

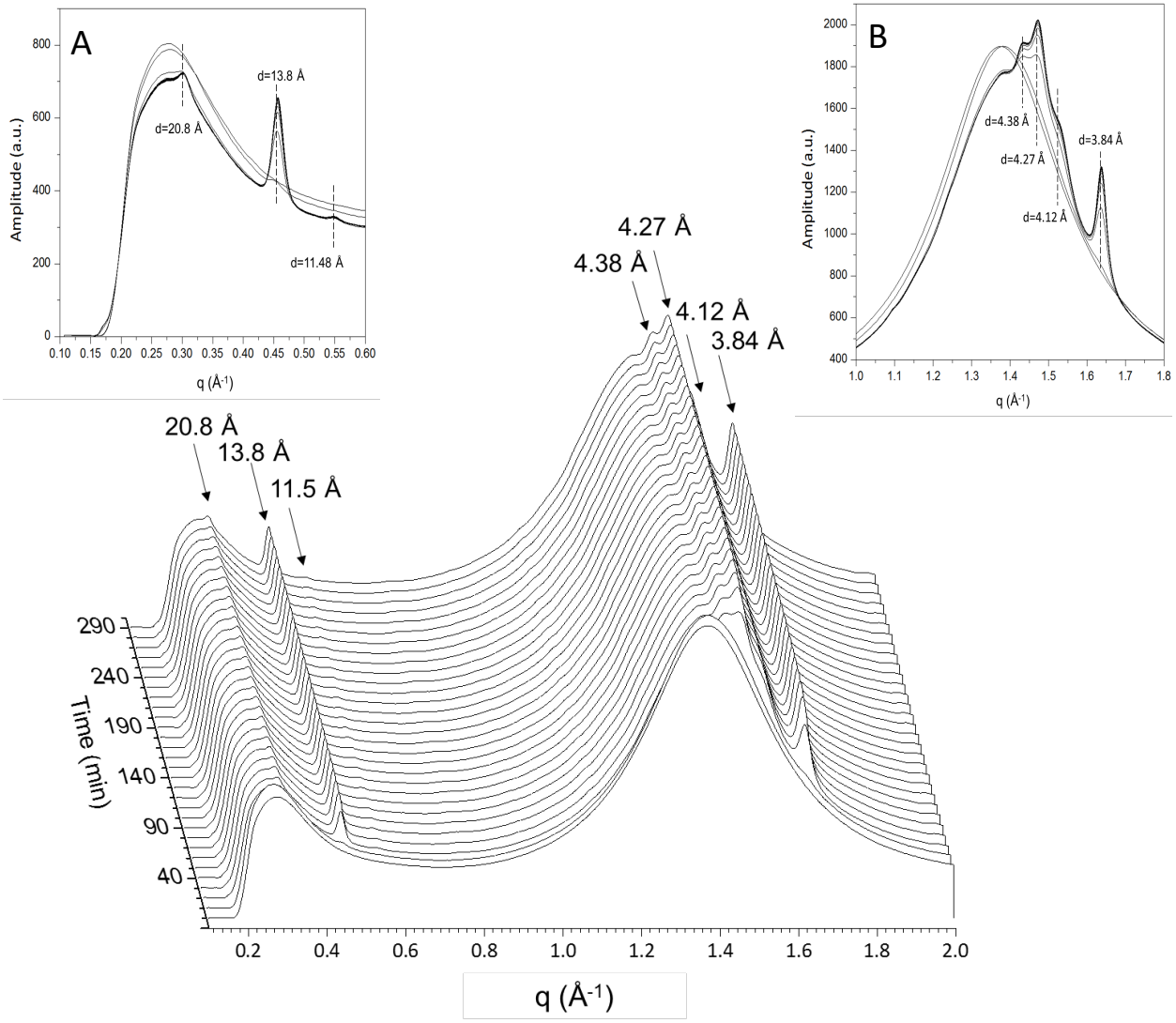
A
d=13.8 Å
d=20.8 Å
d=11.48 Å
Amplitude (a.u.)
q (Å-1)
B
d=4.38 Å
d=4.27 Å
d=4.12 Å
d=3.84 Å
Amplitude (a.u.)
q (Å-1)
4.27 Å
4.38 Å
4.12 Å
3.84 Å
20.8 Å
13.8 Å
11.5 Å
Time (min)
q (Å-1)

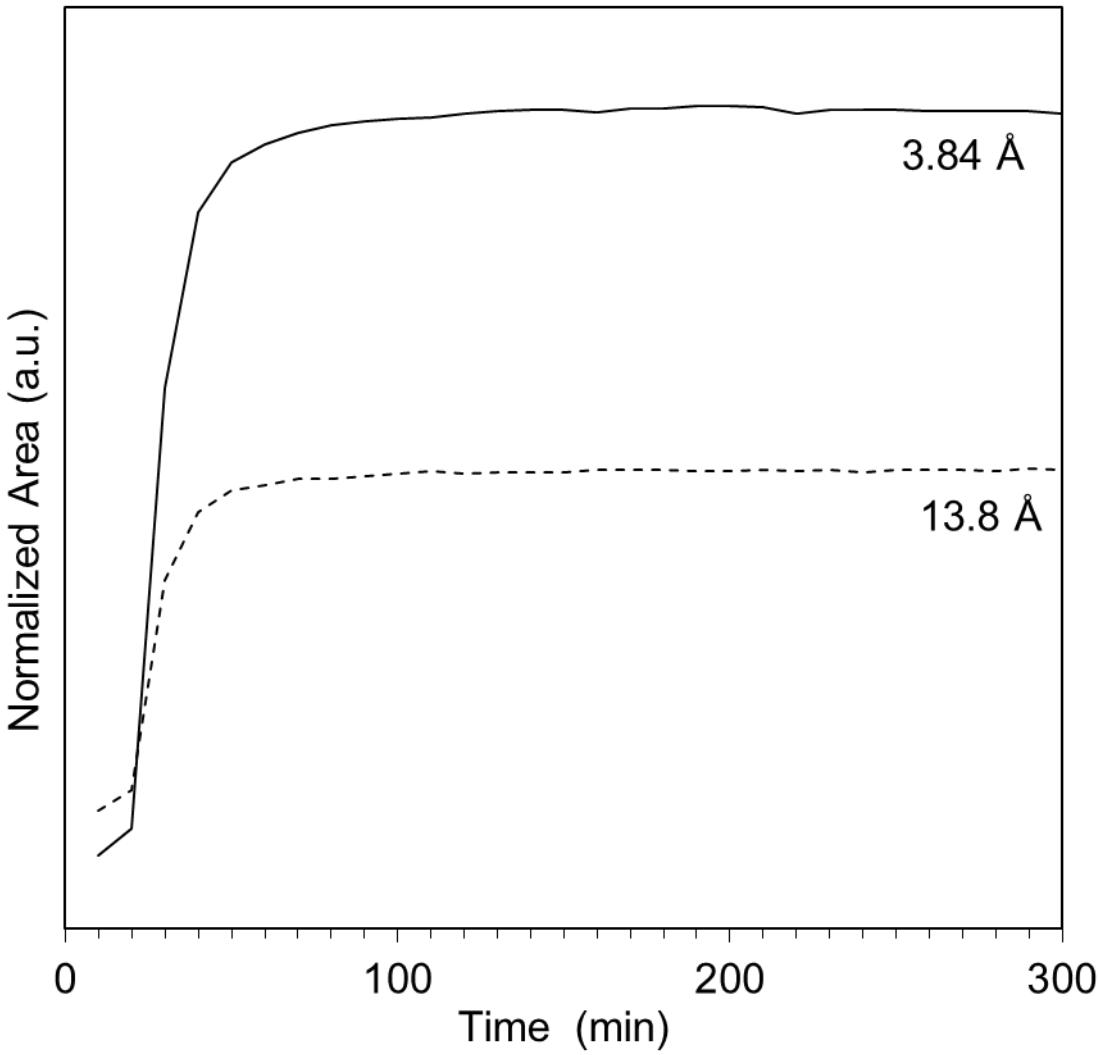
3.84 Å
13.8 Å
Normalized Area (a.u.)
0
100
200
300
Time (min)

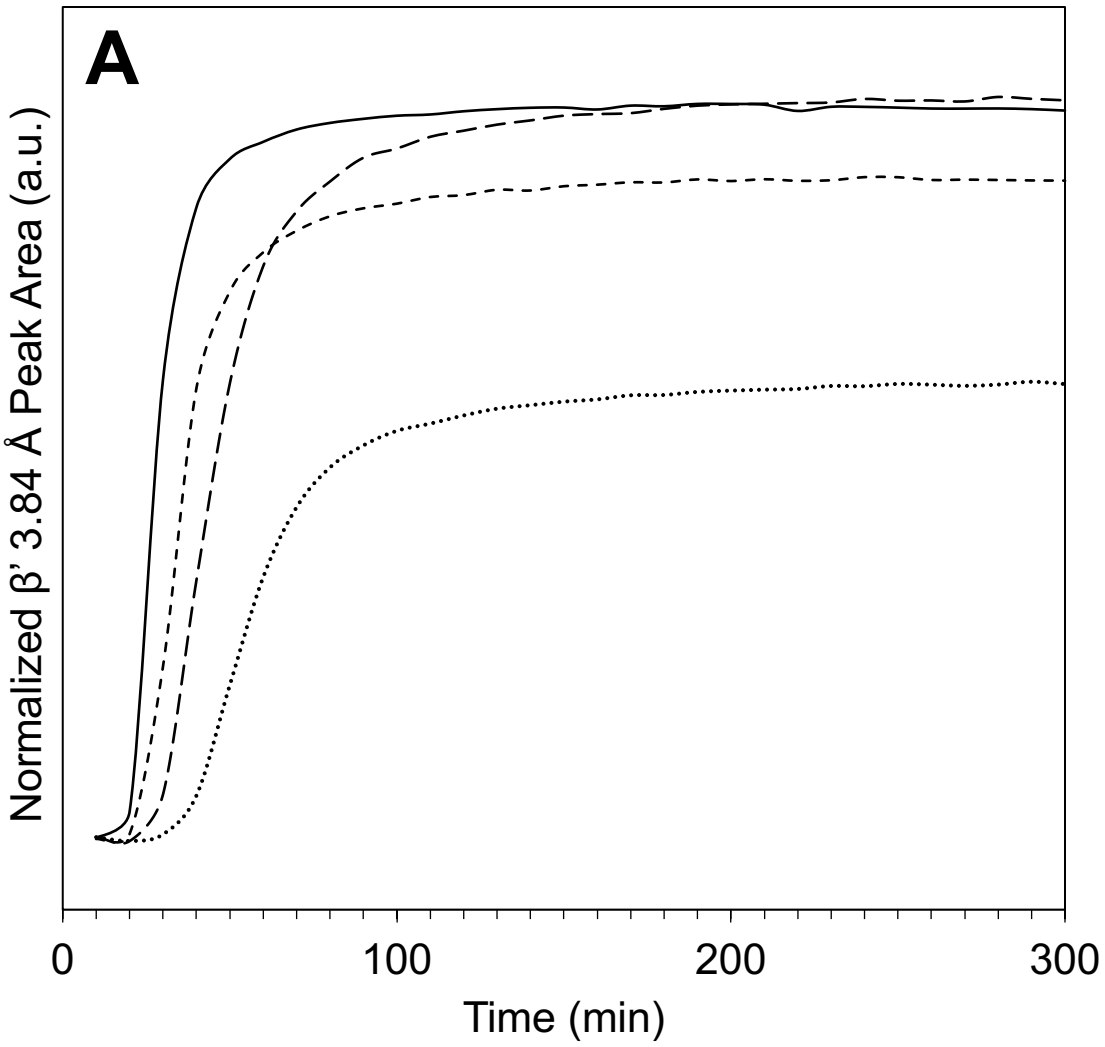
A
Normalized β' 3.84 Å Peak Area (a.u.)
0
100
200
300
Time (min)

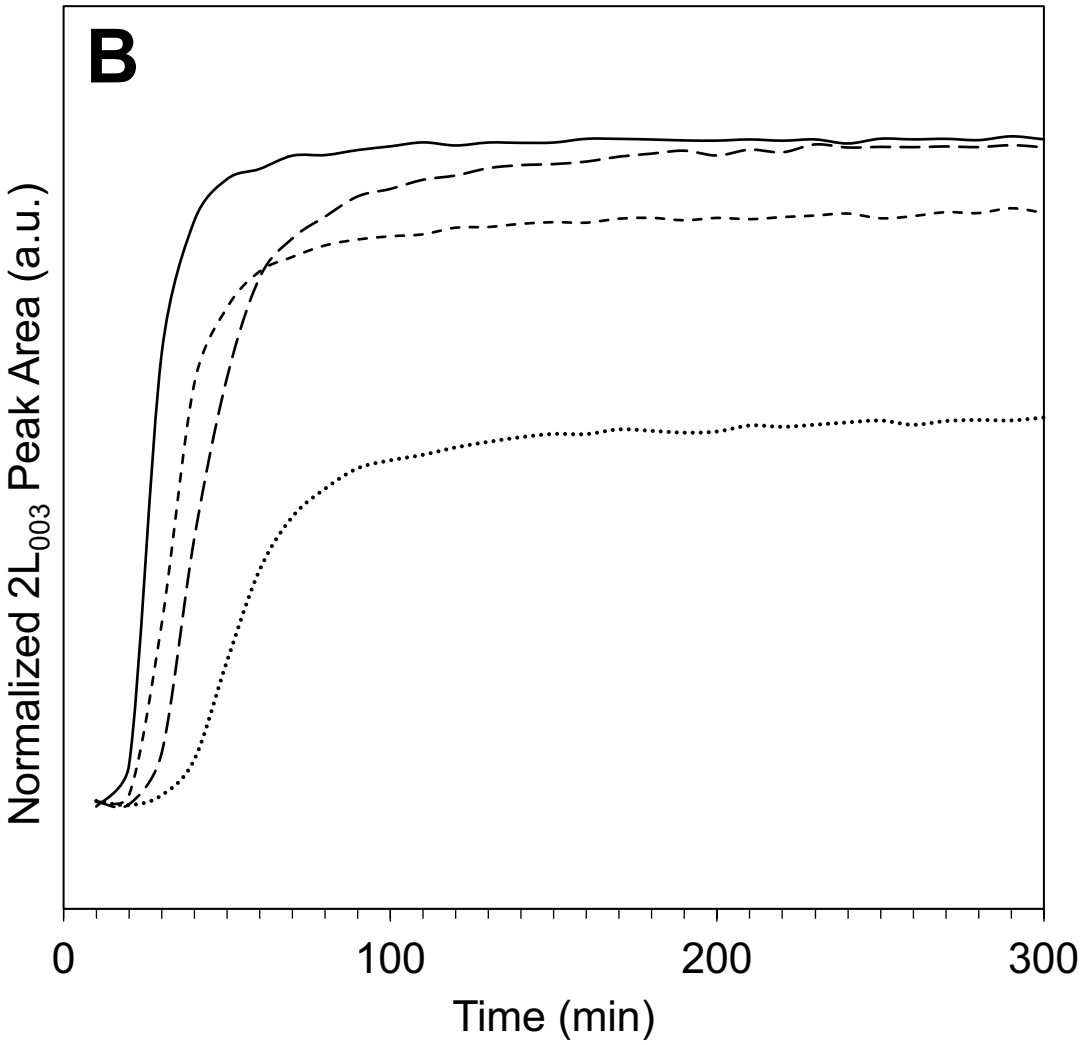
B
Normalized 2L003 Peak Area (a.u.)
0
100
200
300
Time (min)

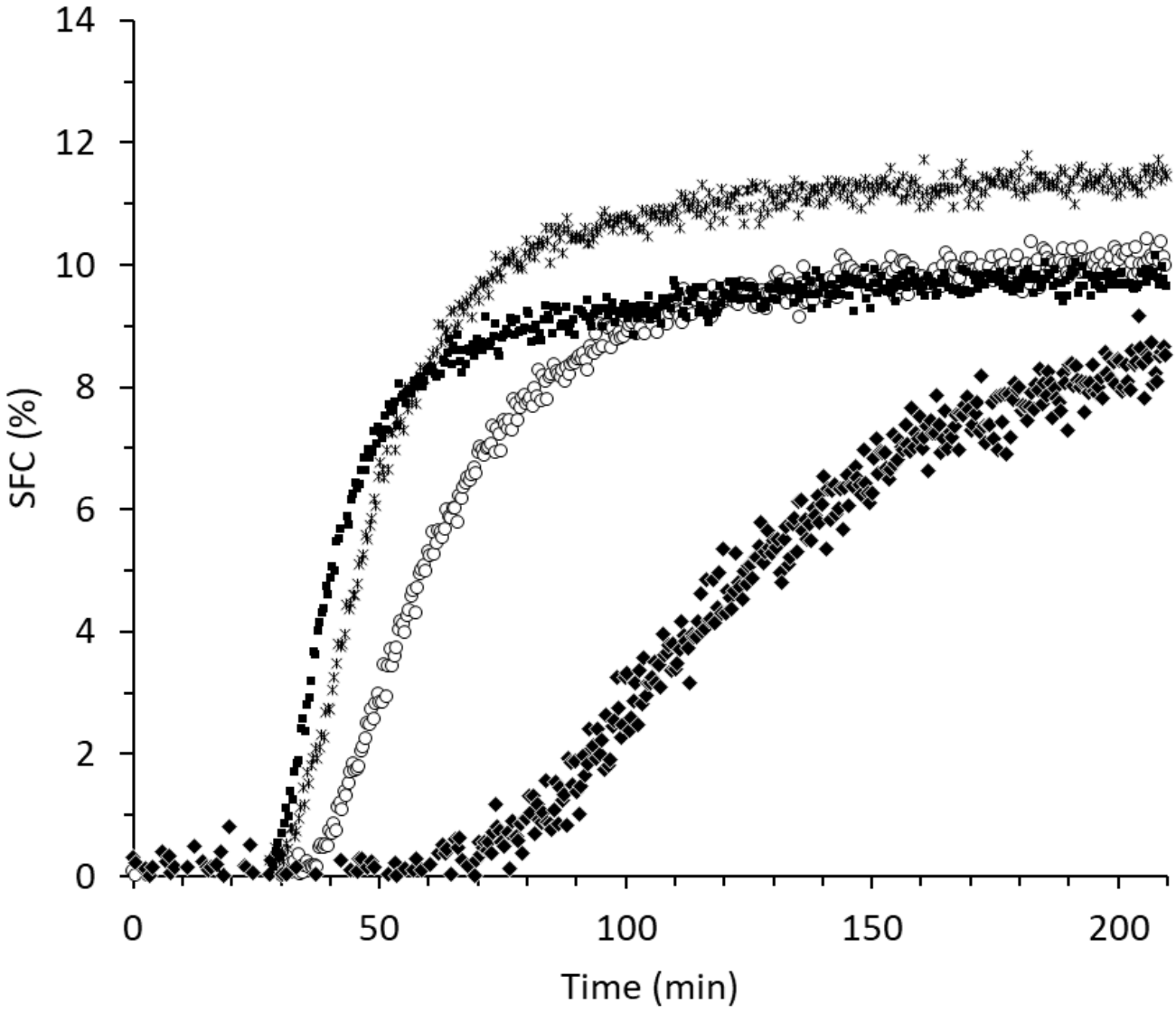
14
12
10
8
6
4
2
0
SFC (%)
0
50
100
150
200
Time (min)

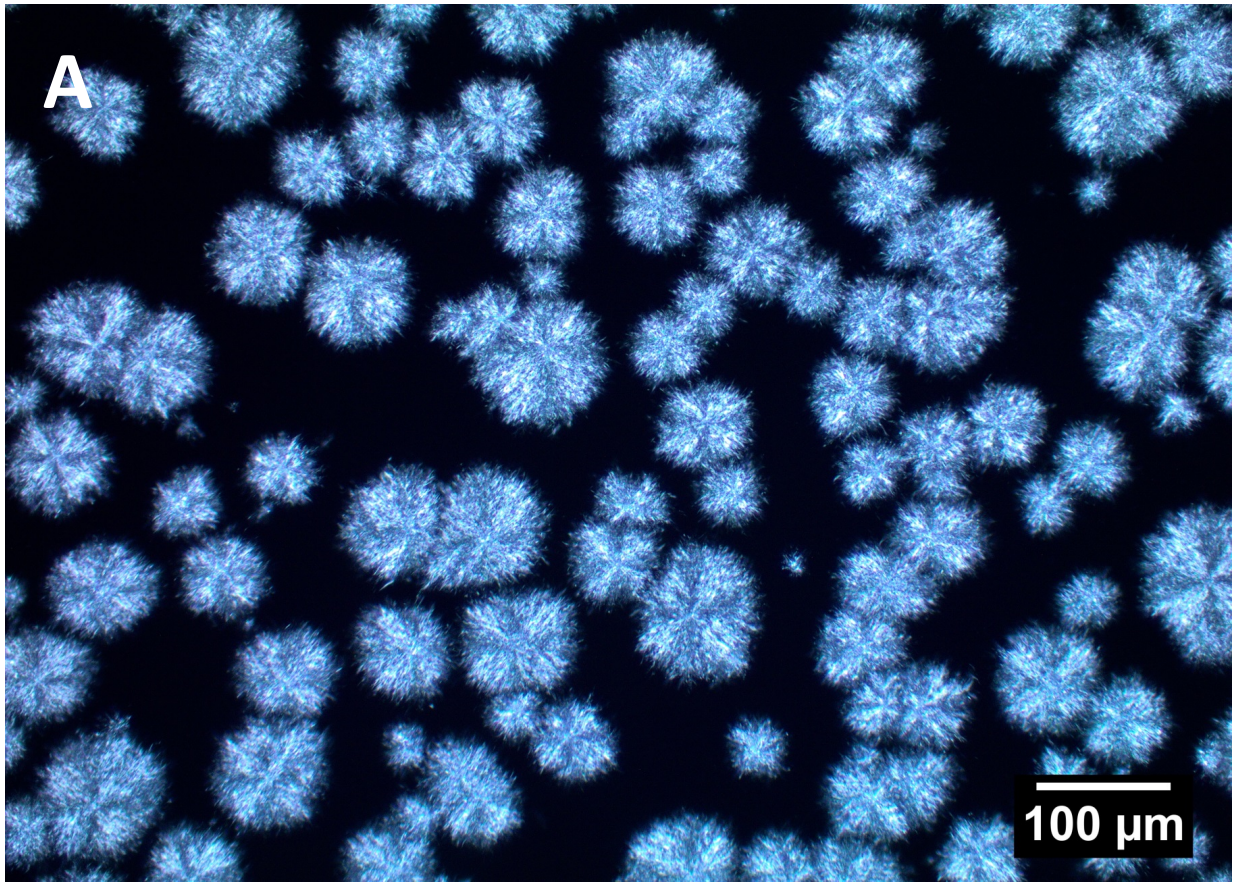
A
100 µm

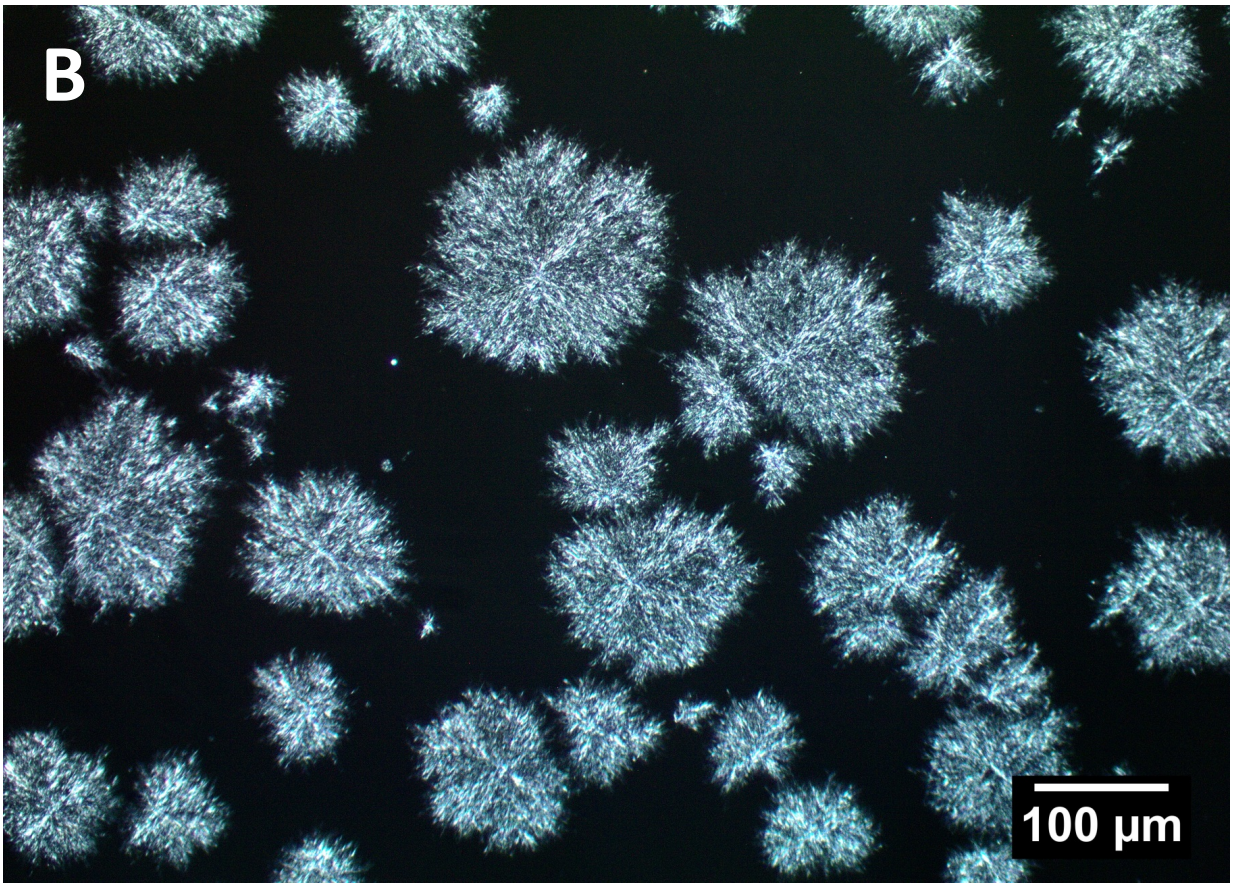
B
100 µm

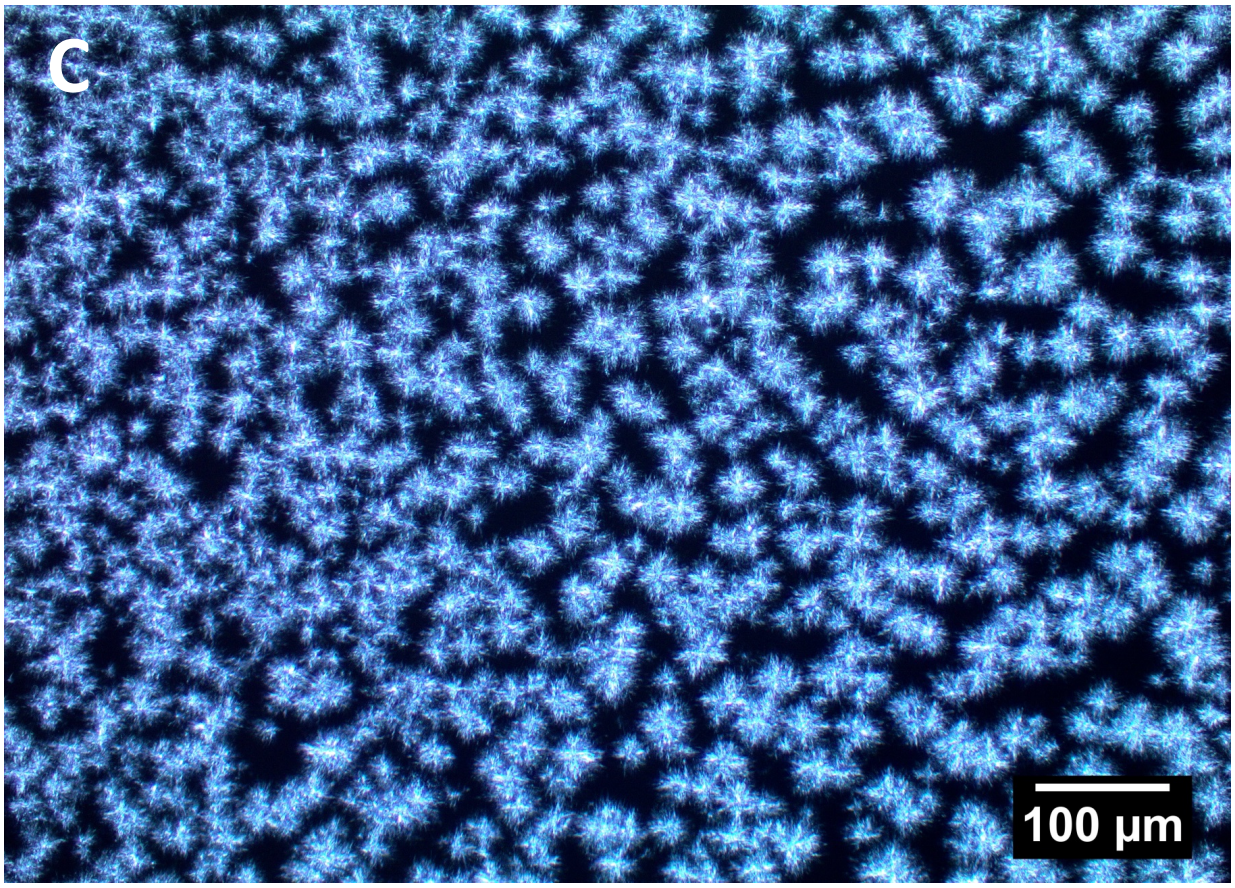
C
100 µm

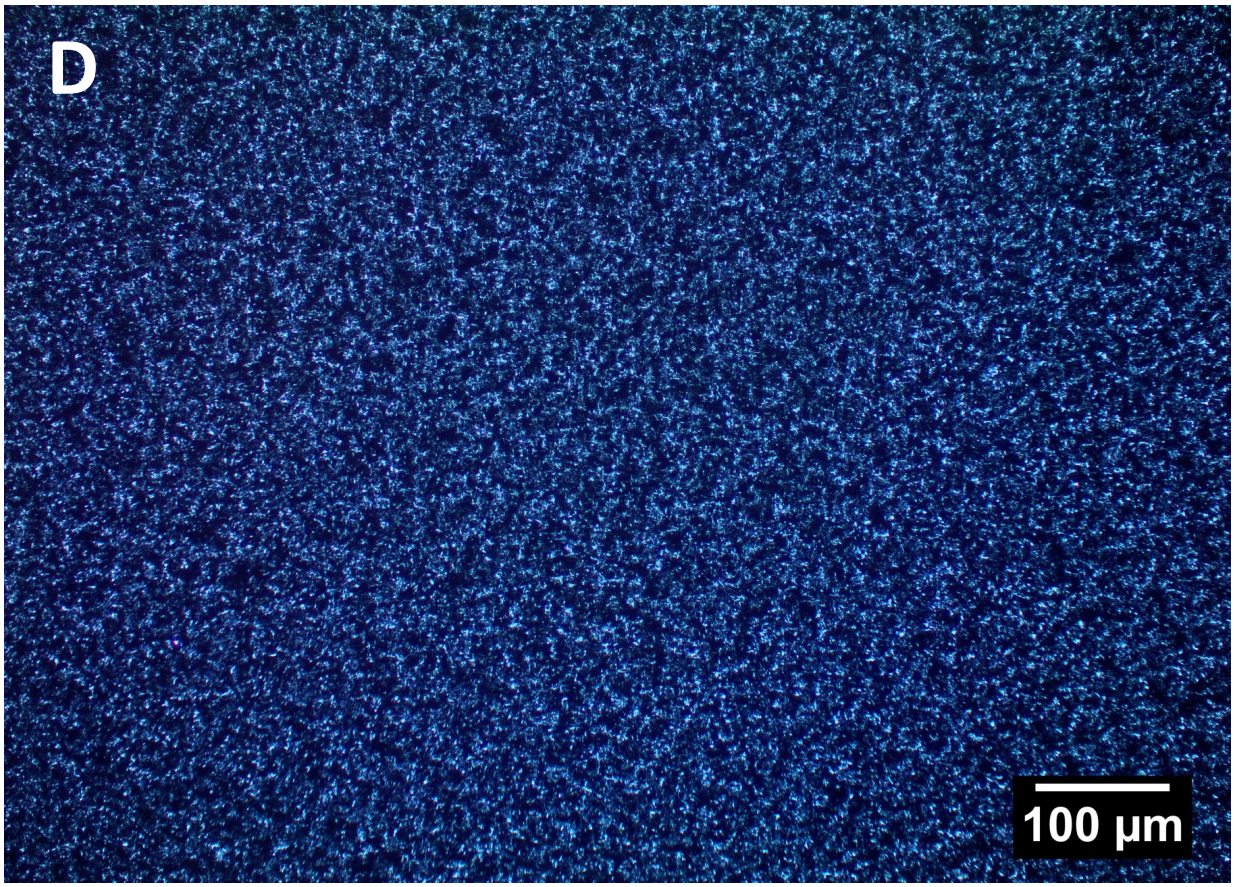
D
100 µm

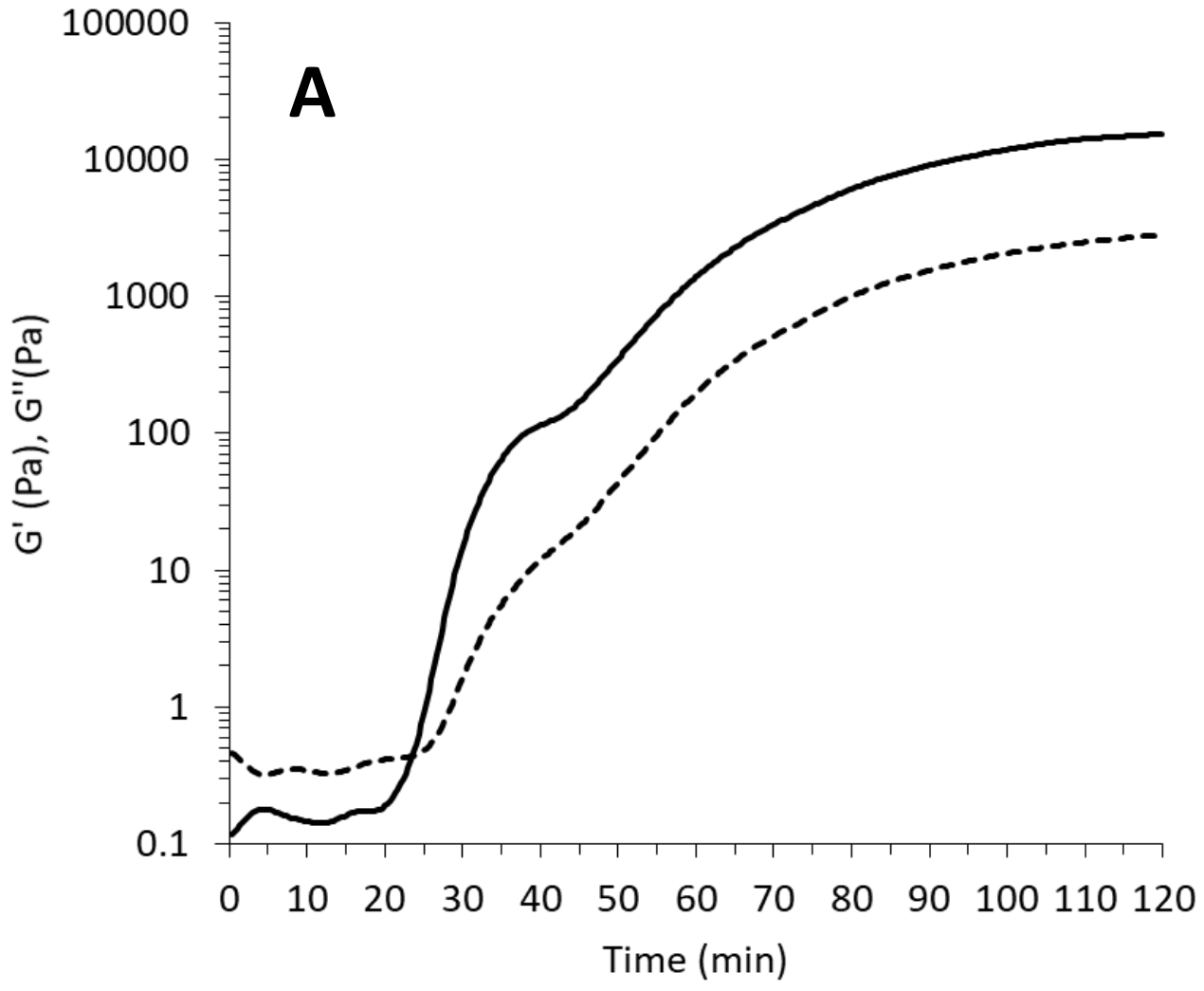
A
100000
10000
1000
100
10
1
0.1
G' (Pa), G''(Pa)
0
10
20
30
40
50
60
70
80
90
100
110
120
Time (min)

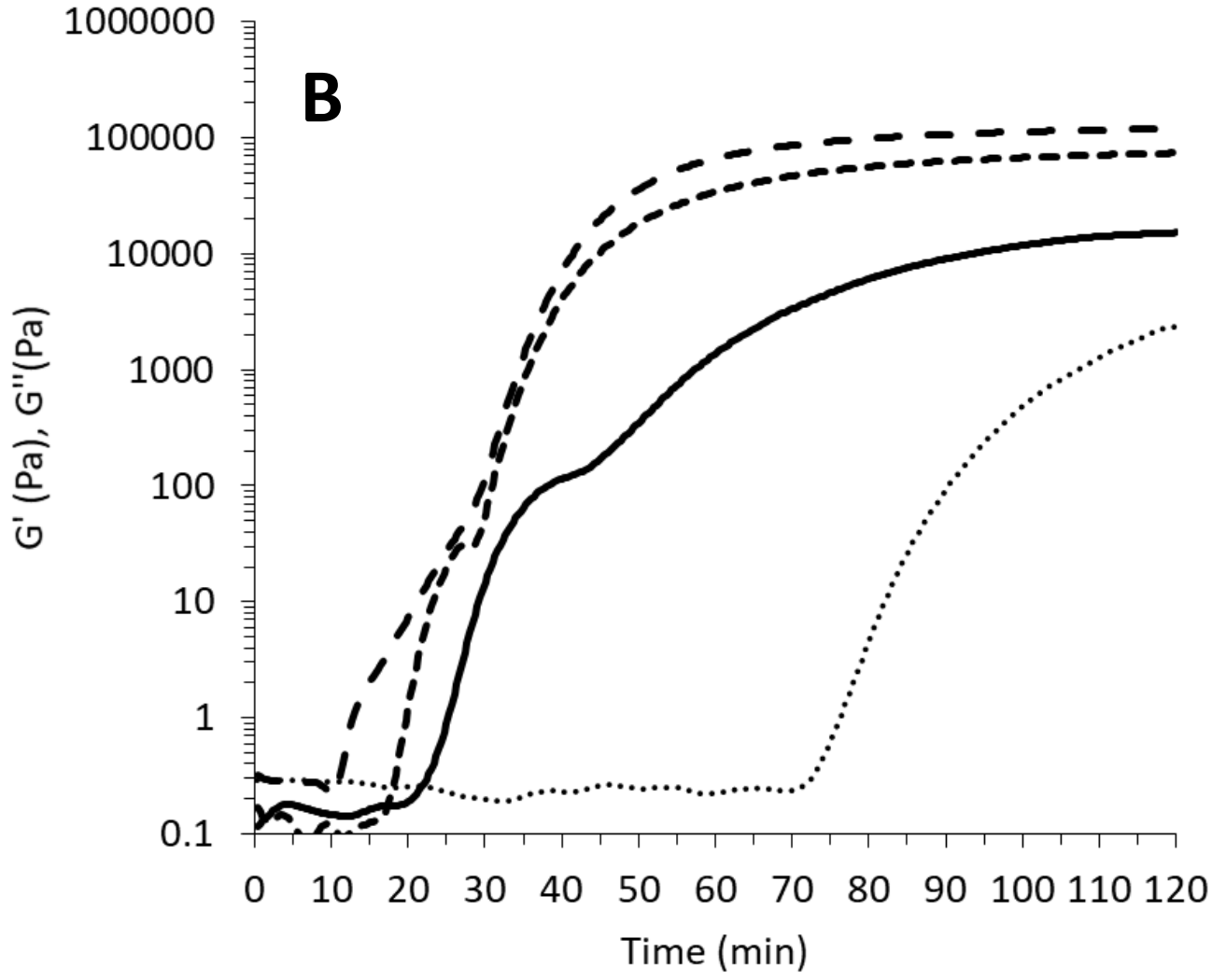
B
1000000
100000
10000
1000
100
10
1
0.1
G' (Pa), G''(Pa)
0
10
20
30
40
50
60
70
80
90
100
110
120
Time (min)